

Article

Preparation of Magnetic g-C₃N₄/Fe₃O₄ Composite and Its Application in the Separation of Catechol from Water

Ruilan Xu and Yong Peng * 

School of Science, Nanchang Institute of Technology, Nanchang 330099, China

* Correspondence: pengyong@nit.edu.cn

Received: 7 August 2019; Accepted: 2 September 2019; Published: 4 September 2019



Abstract: Catechol has strong toxicity and deformity as well as carcinogenicity, and it is difficult to degrade naturally. Therefore, it is of great practical significance to develop efficient adsorbents to separate catechol from water quickly and effectively. In this work, g-C₃N₄/Fe₃O₄ magnetic nanocomposites were prepared using g-C₃N₄ as the matrix by chemical co-precipitation, mixing with Fe²⁺ and Fe³⁺ solutions. Then, g-C₃N₄/Fe₃O₄ was used, for the first time, as an adsorbent to investigate the removal rate of catechol under different conditions by the magnetic field separation method. The adsorption parameters of the g-C₃N₄/Fe₃O₄ nanocomposite were evaluated by the Langmuir and Freundlich adsorption models. The results showed that the g-C₃N₄/Fe₃O₄ nanocomposite presented a two-step adsorption behavior and a considerably high adsorption capacity. The removal rate of catechol reached 70% at the dosage of 50 mg, adsorption time of 30 min, and pH value of 6. Five adsorption–desorption cycles demonstrated that the g-C₃N₄/Fe₃O₄ material had good stability and reusability.

Keywords: catechol; g-C₃N₄; chemical co-precipitation; magnetic separation; adsorption

1. Introduction

Catechol (1,2-dihydroxybenzene) is an important chemical product, which is used widely as the intermediate of fine chemicals such as pesticides, pharmaceuticals, and dyes. Moreover, catechol is also an important intermediate product of phenolic degradation. These are the main reasons why catechol has become an important component of pollutants in environmental water [1]. Due to its strong toxicity, deformity, and carcinogenicity, catechol has been included in the list of priority pollutants in many countries [2–4]. Furthermore, catechol is difficult to degrade, so conventional water treatment technology cannot effectively remove it from polluted water [5]. Currently, the common methods for the removal of catechol include catalytic degradation [6,7], advanced oxidation technology [8–11], and adsorption [12]. Thereinto, adsorption has become a widely used method for the treatment of catechol due to its simple operation, low cost, and high efficiency. Now, many materials are used as adsorbents to remove catechol from water such as activated carbon [12,13], dolomite [14], montmorillonite [15], hydroxyapatite [16], organophilic-bentonite [17], hematite [18], goethite [19], rutile TiO₂ [20], α-alumina [21], magnetic vermiculite [22], resin [23], and waste Fe(III)/Cr(III) hydroxide [24]. These aforementioned materials were modified to increase the pore structure, specific surface area, or special functional groups, thereby enhancing their adsorption effect. Although these modified adsorbents presented good adsorption effect, they were still found to have some disadvantages, for example, high-cost materials, long adsorption time, difficult separation, regeneration, and so on. In order to remove catechol from water easily and effectively, a good adsorbent is still needed [14,15]. Therefore, it is of great significance to develop a new adsorbent with special properties for the rapid separation of catechol in water.

In recent years, the research and development of non-metallic materials such as carbon materials represented by graphene and graphene oxides as well as carbon and nitrogen materials represented by carbon nitride and nitrogen-doped graphene have received great attention. Thereinto, g-C₃N₄ (i.e., graphite-phase C₃N₄) is of particular interest. Its unique two-dimensional Graph-like layered stacking structure and sp² hybrid π conjugated electron band structure can form strong interactions with analytes such as hydrogen bonds, π - π stacking, electrostatic interactions, Van der Waals forces, and hydrophobic effects, which guarantee g-C₃N₄ as an excellent adsorbent [25–27]. However, g-C₃N₄ cannot be used directly as an adsorbent because it is prone to reagglomeration when separated from homogeneous solutions. In addition, the good dispersion of g-C₃N₄ nanomaterials makes separation and recycling difficult [28]. g-C₃N₄/Fe₃O₄ magnetic nanocomposite prepared by grafting Fe₃O₄ onto C₃N₄ has good stability, large surface area, and good water solubility. It can also hopefully be used as a solid phase extraction adsorbent, separating the target objects from solutions quickly by an external magnetic field. This will greatly simplify cumbersome procedures such as centrifugation and filtration, thus exhibiting significant practical significance. The reported methods of the preparation of g-C₃N₄/Fe₃O₄ composite contain chemical co-precipitation [28–30], the solvothermal method [27,31], and simple physical blending [32]. Wang et al. [28] successfully prepared g-C₃N₄/Fe₃O₄ nanocomposites by chemical co-precipitation, which was used as a solid phase extraction adsorbent for the first time to separate and enrich polycyclic aromatic hydrocarbons (PAHs) in environmental water. The detection limit of this method was 0.05–0.1 $\mu\text{g/L}$, the precision was 1.8–5.3%, and the recovery rate was 80.0–99.8%. Zheng et al. [32] developed a solid-phase microextraction method based on magnetic g-C₃N₄ nanosheets, which were further applied for the determination of PAHs in different edible oil samples coupled with GC/MS analysis. Limits of quantitation for the eight PAHs ranged from 0.4 to 0.9 ng/g. The recoveries ranged from 91.0% to 124.1%, with RSDs of less than 10.2%.

In this work, g-C₃N₄ was prepared by thermal polymerization with melamine as the precursor. Then, g-C₃N₄/Fe₃O₄ magnetic nanocomposites were prepared by the chemical co-precipitation of g-C₃N₄ with FeCl₃·6H₂O and FeSO₄·7H₂O solutions in a certain proportion. The removal rates of catechol by g-C₃N₄/Fe₃O₄ magnetic composite were investigated under different g-C₃N₄/Fe₃O₄ dosage, adsorption time, and pH value. The stability and reusability of the composites were evaluated by adsorption–desorption cycle experiments.

2. Materials and Methods

2.1. Materials

Melamine ($\geq 99.0\%$), FeCl₃·6H₂O ($\geq 99.0\%$), FeSO₄·7H₂O (99.0~101.0%), concentrated ammonia water (25.0~28.0%), anhydrous ethanol ($\geq 99.7\%$), isopropanol ($\geq 99.7\%$), and acetic acid ($\geq 99.8\%$) were purchased from Sinopharm Chemical Reagent Co. Ltd. (Shanghai, China). Acetonitrile (99.9%), methanol (99.9%), and catechol (99%) were obtained from J&K Co. Ltd. (Beijing, China). All other solvents were of HPLC or analytical grade. Deionized water was used in all experiments.

2.2. Preparation of Catechol Stock Solution

A concentration of 1 g/L stock solution of catechol was prepared by dissolving catechol (99%) in deionized water, then transferred into a brown bottle, and reserved in a refrigerator for later use. Working solutions were prepared daily by diluting the stock solution with deionized water.

2.3. Preparations of g-C₃N₄, Fe₃O₄ and g-C₃N₄/Fe₃O₄

g-C₃N₄ was prepared at 520 °C for 4 h in a N₂ atmosphere by thermal polymerization using melamine as the precursor, with the heating rate of 4 °C/min. After cooling, a pale yellow powder g-C₃N₄ was obtained by grinding. g-C₃N₄/Fe₃O₄ was prepared by chemical co-precipitation [28–30]. According to a typical procedure, g-C₃N₄ (1.860 g) was dispersed in 40.0 mL brown-yellow solution mixed of FeCl₃·6H₂O (0.540 g) and FeSO₄·7H₂O (0.278 g) and then ultrasonically dispersed for 30 min

at room temperature. The resulting orange-yellow suspension was transferred to a three-necked flask in a N₂ atmosphere at 70 °C with magnetic stirring for 1 h. Next, the ammonia solution was injected into the reaction mixture until the pH reached 10.0. The resulting mixture was stirred at 70 °C for another 1 h, after which the reaction mixture was cooled and washed several times with ethanol and deionized water. The nanocomposite was dried in a vacuum oven at 40 °C for 12 h.

In order to better characterize and prove the structure of g-C₃N₄/Fe₃O₄, the Fe₃O₄ nanoparticles were prepared by chemical co-precipitation similar to the preparation of g-C₃N₄/Fe₃O₄. FeCl₃·6H₂O (4.066 g) and FeSO₄·7H₂O (2.107 g) were dissolved in 80 mL water ultrasonically at room temperature and then transferred into a three-necked flask in a N₂ atmosphere at 70 °C with magnetic stirring for 1 h. Next, the ammonia solution was injected into the reaction mixture until the pH reached 10.0. The resulting mixture was stirred at 70 °C for another 1 h, after which the reaction mixture was cooled and washed several times with deionized water. The nanoparticle was dried in a vacuum oven at 40 °C for 12 h.

2.4. Characterizations of g-C₃N₄, Fe₃O₄ and g-C₃N₄/Fe₃O₄

X-ray diffraction (XRD) was carried out on Bruker D8 Advance Diffraction Instrument (Bruker, Karlsruhe, Germany) in the range of 10°–80° at a scanning rate of 5°/min under 40 kV. Scanning electron microscopy (SEM) and transmission electron microscopy (TEM) were executed on a JEOL JSM-6701F (JEOL, Tokyo, Japan) and JEM-2100 (Hitachi, Tokyo, Japan), respectively. The Fourier transform infrared (FT-IR) spectrum was obtained from a Thermo Fisher Nicolet iS10 (Thermo Fisher Scientific, Waltham, MA, USA) in the range of 400–4000 cm⁻¹ with KBr pellets. Nitrogen adsorption–desorption isotherms were measured on a Micromeritics ASAP 2020 (Micromeritics, Norcross, GA, USA). Magnetic characterization was carried out using a Physical Property Measurement System (PPMS-9, Quantum design, San Diego, CA, USA) with fields up to 20,000 Oe at the temperature of 300 K.

2.5. Adsorption Properties of g-C₃N₄/Fe₃O₄

Adsorption isotherms of catechol onto g-C₃N₄/Fe₃O₄ surfaces were carried out in a capped centrifugal tube at 308 K with pH 6 by ultrasonic adsorption. A series of catechol solutions with concentrations from 6 mg/L to 300 mg/L were prepared from a stock solution of 1 g/L. The pH of the solutions was adjusted with acetic acid and ammonia solution. A total of 50 mg of the g-C₃N₄/Fe₃O₄ composites were added into 5 mL catechol standard solutions with initial concentrations as above, respectively, followed by ultrasonic adsorption for 30 min in room temperature. An external magnetic field was used to separate the g-C₃N₄/Fe₃O₄ nanocomposites from the catechol supernatant (as shown in Figure 1). The concentration of catechol solution was determined by an Ultraviolet-Visible spectrophotometer (UV-1810S, Yoke, Shanghai, China) with the maximum absorption wavelength of 275 nm.

The adsorption properties of the g-C₃N₄/Fe₃O₄ nanocomposites on catechol were investigated under different g-C₃N₄/Fe₃O₄ dosage, adsorption time, and pH values (as shown in Table 1). The removal rate (η) and adsorption capacity (Q_e) was calculated according to the difference between the initial concentration of catechol and the concentration of catechol in the supernatant at adsorption equilibrium. The calculation formula is as follows:

$$\eta = (C_0 - C_e)/C_0 \times 100\% \quad (1)$$

$$Q_e = (C_0 - C_e)V/m \quad (2)$$

where C_0 and C_e (mg/L) are the initial concentration of catechol in water and the concentration of catechol in the supernatant at adsorption equilibrium, respectively. m (mg) is the dosage of g-C₃N₄/Fe₃O₄ and V (mL) is the volume of the aqueous solution.

Acetonitrile, methanol, and isopropanol were chosen as desorption agents to study the effects on the recovery of catechol from g-C₃N₄/Fe₃O₄ nanocomposites under the optimum adsorption

conditions. A total of 5 mL of the three desorption solvents above-mentioned were added with ultrasonic desorption for 20 min. Five adsorption and desorption experiments were repeated to test the stability and reusability of the g-C₃N₄/Fe₃O₄ nanocomposite. The concentration of catechol in the supernatant after desorption was determined to be C_d (mg/L), and the formula for calculating the recovery rate of catechol was as follows:

$$\delta = C_d / (10 - C_e) \times 100\% \quad (3)$$

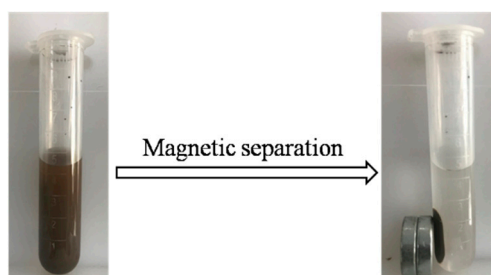


Figure 1. Separation of the supernatant by an external magnetic field.

Table 1. Experimental conditions during the adsorption of catechol.

| Experimental Conditions | Concentration of Catechol (mg/L) | g-C ₃ N ₄ /Fe ₃ O ₄ Dosage (mg) | Adsorption Time (min) | pH Value |
|---|---|---|-----------------------|------------------|
| Concentration of catechol (mg/L) | 6, 10, 14, 20, 25, 30, 40, 50, 100, 200, 300, 400, 500, 600 | 50 | 30 | 6 |
| g-C ₃ N ₄ /Fe ₃ O ₄ dosage (mg) | 10 | 12.5, 25, 37.5, 50, 75 | 30 | 7 |
| Adsorption time (min) | 10 | 50 | 5, 10, 20, 30, 40 | 7 |
| pH value | 10 | 50 | 30 | 4, 5, 6, 7, 8, 9 |

2.6. Adsorption Isotherms

The adsorption isotherms were subjected to analysis in terms of the well-known Langmuir and Freundlich adsorption models.

The Langmuir equation can be represented by [33]:

$$C_e/Q_e = 1/(Q_m \cdot K_L) + C_e/Q_m \quad (4)$$

where C_e (mg/L) is the concentration of catechol at equilibrium; Q_e (mg/g) is the equilibrium amount of catechol adsorbed; K_L (L/mg) is a constant related to the intensity of adsorption; and Q_m (mg/g) is the maximum amount adsorbed for a complete monolayer coverage.

The equation of the Freundlich isotherm can be written as [34]:

$$\log Q_e = \log K_F + (1/n) \cdot \log C_e \quad (5)$$

where K_F (L/mg) and n are the Freundlich constants related to the adsorption capacity and the intensity of adsorption, respectively.

3. Results and Discussion

3.1. Characterizations

Figure 2 shows the SEM images of g-C₃N₄ (a), Fe₃O₄ (b), g-C₃N₄/Fe₃O₄ (c), and TEM images of g-C₃N₄ (d), Fe₃O₄ (e), and g-C₃N₄/Fe₃O₄ (f). As shown in Figure 2a,d, g-C₃N₄ prepared by melamine

had a lamellar structure with a relatively smooth surface. Figure 2b,e shows that most of the Fe_3O_4 nanoparticles were spherical and uniform in size, with an average particle size of about 20 nm, but poorly dispersed. Figure 2c,f shows that Fe_3O_4 particles were successfully loaded onto the lamellar structure of $\text{g-C}_3\text{N}_4$, forming a $\text{g-C}_3\text{N}_4/\text{Fe}_3\text{O}_4$ composite system.

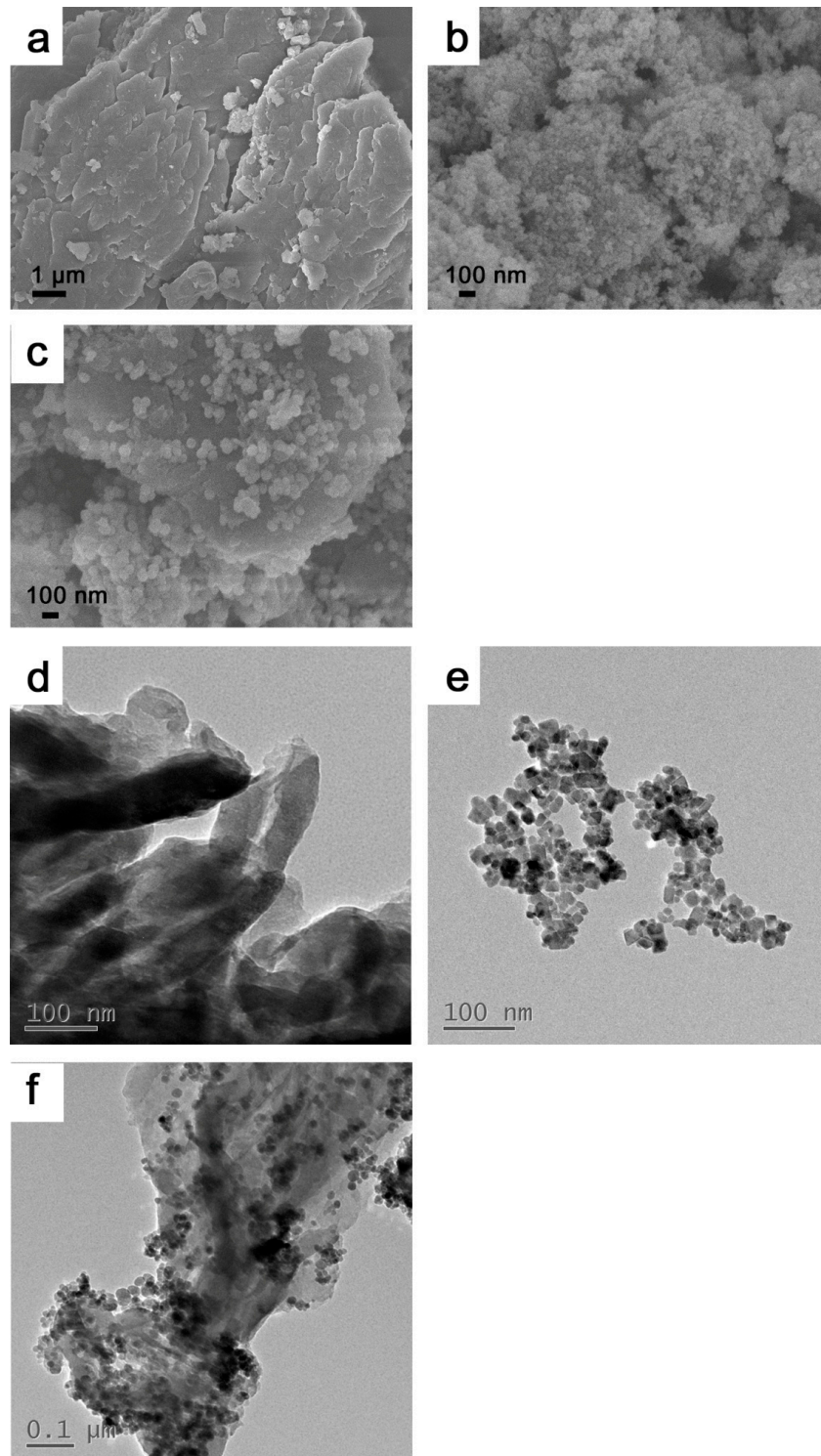


Figure 2. Scanning electron microscopy (SEM) images of $\text{g-C}_3\text{N}_4$ (a), Fe_3O_4 (b), and $\text{g-C}_3\text{N}_4/\text{Fe}_3\text{O}_4$ (c), and transmission electron microscopy (TEM) images of $\text{g-C}_3\text{N}_4$ (d), Fe_3O_4 (e), and $\text{g-C}_3\text{N}_4/\text{Fe}_3\text{O}_4$ (f).

Figure 3 shows the XRD patterns of $g\text{-C}_3\text{N}_4$ (a), Fe_3O_4 (b), and $g\text{-C}_3\text{N}_4/\text{Fe}_3\text{O}_4$ (c). According to the literature [28,30], the XRD spectra of pure $g\text{-C}_3\text{N}_4$ has two characteristic peaks at $2\theta = 27.4^\circ$ and $2\theta = 13.1^\circ$. Therefore, the strong peak at 27.4° can be attributed to the typical (002) interlayer diffraction peak, while the peak at 13.1° belongs to the (100) crystal plane diffraction peak accumulated in the interlayer structure. As shown in Figure 3a, the characteristic peaks of $g\text{-C}_3\text{N}_4$ prepared by melamine were consistent with the data stated above and the crystal database JCPDS 87-1526, with no other impurity peaks, indicating that $g\text{-C}_3\text{N}_4$ was successfully prepared. In Figure 3b, six characteristic diffraction peaks of (220), (311), (400), (440), (422), (511), and (440) could be observed at the 2θ degree of 30.2° , 35.6° , 43.3° , 53.5° , 57.1° , and 62.7° , respectively, which are in accordance with the standard Fe_3O_4 crystal data (JCPDS 19-0629) and literature description [28,30]. The diffraction peaks identified that the Fe_3O_4 had a face-centered-cubic structure [29]. In Figure 3c, both of the aforementioned characteristic diffraction peaks of $g\text{-C}_3\text{N}_4$ and Fe_3O_4 appeared in one XRD pattern at the same time, indicating that material c was a two-phase composite composed of $g\text{-C}_3\text{N}_4$ and Fe_3O_4 . Furthermore, the intensity of the Fe_3O_4 diffraction peaks in the composite were higher than that in the pure Fe_3O_4 powder. Thus, the dispersion degree of Fe_3O_4 nanoparticles in the composite was significantly improved, which is beneficial for an increase in the adsorption sites and therefore the adsorption capacity.

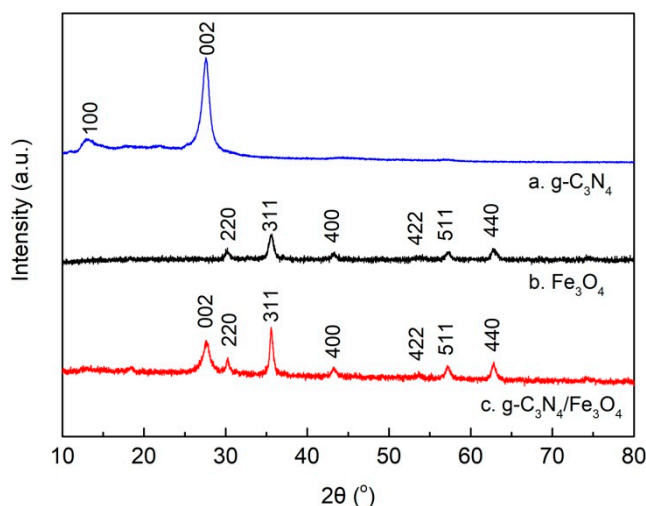


Figure 3. X-ray diffraction (XRD) patterns of $g\text{-C}_3\text{N}_4$ (a), Fe_3O_4 (b), and $g\text{-C}_3\text{N}_4/\text{Fe}_3\text{O}_4$ (c).

Figure 4 shows the IR spectrum of $g\text{-C}_3\text{N}_4$ (a), Fe_3O_4 (b), and $g\text{-C}_3\text{N}_4/\text{Fe}_3\text{O}_4$ (c). In Figure 4a, the broad absorption band at $3100\text{--}3300\text{ cm}^{-1}$ can be attributed to the stretching vibration of N–H in $g\text{-C}_3\text{N}_4$. Absorption peaks at $1640\text{--}1400\text{ cm}^{-1}$ can be assigned to the stretching vibration of repetitive elements in $g\text{-C}_3\text{N}_4$. Absorption peaks at 1332 cm^{-1} and 1244 cm^{-1} are due to the stretching vibration of C–N, and the absorption peaks at 808 cm^{-1} can be attributed to the bending vibration of triazine ring. In Figure 4b, the characteristic absorption peak around 570 cm^{-1} belongs to the stretching vibration of the Fe–O bond in pure Fe_3O_4 , which is in accordance with the data in the literature [28,30]. The IR spectrum of Figure 4c shows that there are absorption peaks corresponding to Figure 4a at $3100\text{--}3300\text{ cm}^{-1}$, $1640\text{--}1400\text{ cm}^{-1}$, 1333 cm^{-1} , 1246 cm^{-1} , and 808 cm^{-1} , indicating that material b is composed of $g\text{-C}_3\text{N}_4$. In addition, the peak at around 570 cm^{-1} was also consistent with the characteristic absorption peak of Fe–O in Fe_3O_4 , which further proved that the $g\text{-C}_3\text{N}_4/\text{Fe}_3\text{O}_4$ composite was successfully prepared.

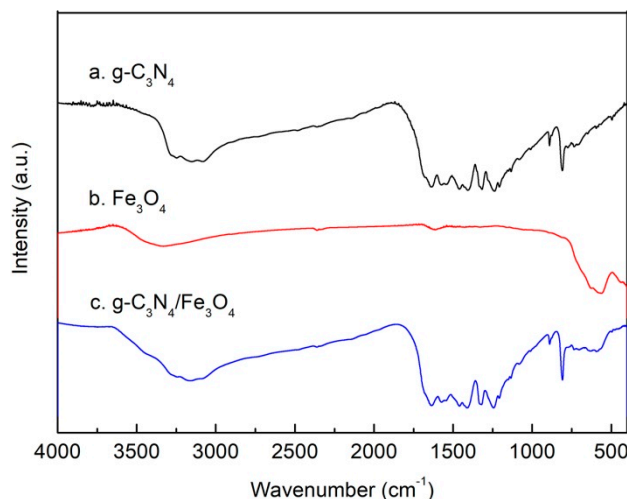


Figure 4. IR spectrum of g-C₃N₄ (a), Fe₃O₄ (b), and g-C₃N₄/Fe₃O₄ (c).

Nitrogen adsorption–desorption measurements (Figure 5) were performed to investigate the Brunauer-Emmett-Teller (BET) surface area (S_{BET}), pore volume and dimension of pure g-C₃N₄ and g-C₃N₄/Fe₃O₄ composite. These textural properties are listed in Table 2. As seen from Table 2, the calculated S_{BET} of g-C₃N₄ showed (20.6 m²/g), a considerably high surface area when compared with other reported S_{BET} (8.56 m²/g) of g-C₃N₄ [29]. g-C₃N₄/Fe₃O₄ exhibited a S_{BET} of 38.8 m² g⁻¹, which is higher than that of the pure g-C₃N₄. The pore volume and size were decreased after the introduction of Fe₃O₄, illustrating that the Fe₃O₄ nanoparticles entered into the mesopores inside the g-C₃N₄.

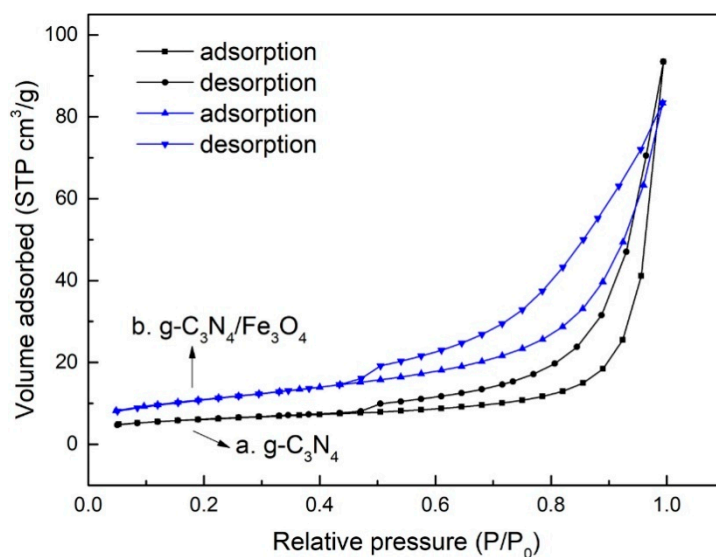


Figure 5. Nitrogen adsorption–desorption isotherm plots for g-C₃N₄ (a) and g-C₃N₄/Fe₃O₄ (b).

Table 2. Textural properties of g-C₃N₄ and the g-C₃N₄/Fe₃O₄ composite.

| Materials | S_{BET} (m ² /g) | Pore Volume (cm ³ /g) | Pore Size (nm) |
|---|--------------------------------------|----------------------------------|----------------|
| g-C ₃ N ₄ | 20.6 | 0.145 | 28.0 |
| g-C ₃ N ₄ /Fe ₃ O ₄ | 38.8 | 0.129 | 13.3 |

The typical magnetization curves of Fe₃O₄ (a) and g-C₃N₄/Fe₃O₄ (b) at 300 K are shown in Figure 6. It can be seen that the saturation magnetization (M_s) values for Fe₃O₄ and g-C₃N₄/Fe₃O₄ were about 66.8 and 17.7 emu/g, respectively, indicating that the g-C₃N₄/Fe₃O₄ composite presented

good magnetic property. Therefore, the $g\text{-C}_3\text{N}_4/\text{Fe}_3\text{O}_4$ particles could be simply and quickly separated from the aqueous solutions by an external magnetic field.

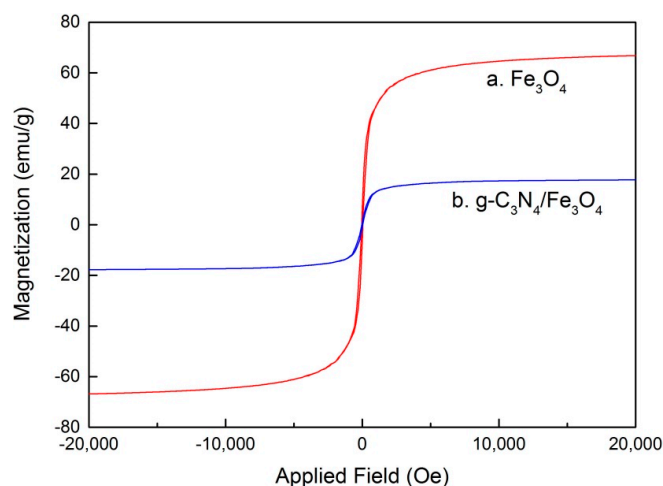


Figure 6. Magnetization curves of Fe_3O_4 (a) and $g\text{-C}_3\text{N}_4/\text{Fe}_3\text{O}_4$ (b).

3.2. Adsorption of Catechol

The adsorption isotherm of catechol on $g\text{-C}_3\text{N}_4/\text{Fe}_3\text{O}_4$ composite was determined by varying the initial catechol concentration at a pH value of 6 and temperature of 308 K. As shown in Figure 7, the isotherm does not exhibit a typical type-I adsorption isotherm, according to the Brunauer classification, but a two-step adsorption behavior can be seen. This may contribute to the two different kinds of adsorption site that exist in the $g\text{-C}_3\text{N}_4/\text{Fe}_3\text{O}_4$ composite, since there are two potential adsorptive phases: the graphite phase and magnetite. Langmuir and Freundlich models were utilized to fit the experimental isotherm data (Figure 7). The extracted values of the adsorption isotherm parameters are summarized in Table 3. The R^2 extracted from both models was higher than 0.98. This means that the correlated isotherms from both models were fairly good. The maximum adsorption amount (Q_{max}) calculated from the Langmuir model was 24.9 mg g^{-1} . The slightly higher R^2 value extracted from the Freundlich model indicates that this model may describe the adsorption behavior of catechol on the $g\text{-C}_3\text{N}_4/\text{Fe}_3\text{O}_4$ composite better. The relatively high value of $1/n$ (0.739) implies that the two possible kinds of adsorption sites are mainly homogeneous.

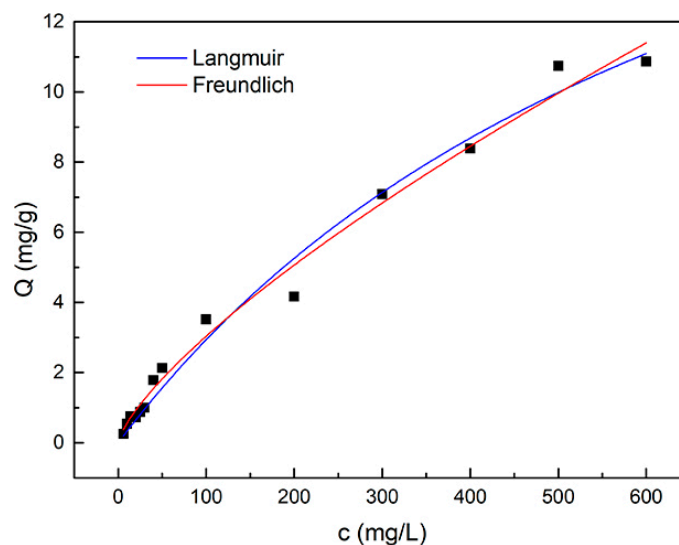
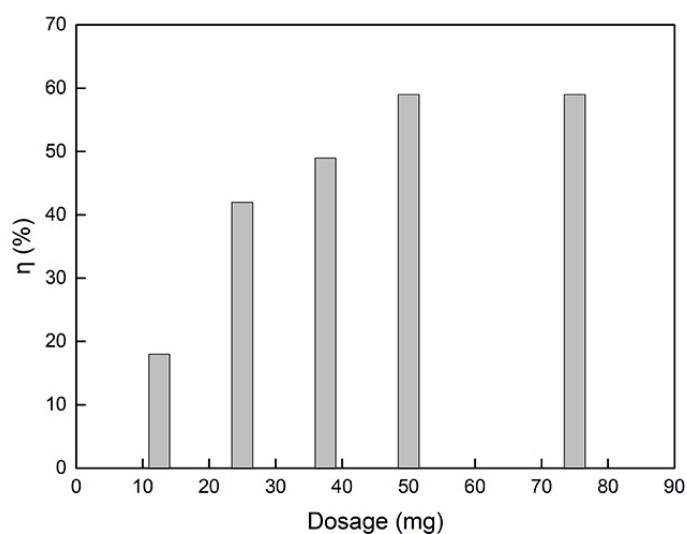


Figure 7. Adsorption isotherms of catechol on the $g\text{-C}_3\text{N}_4/\text{Fe}_3\text{O}_4$ composite. Lines are the model correlations.

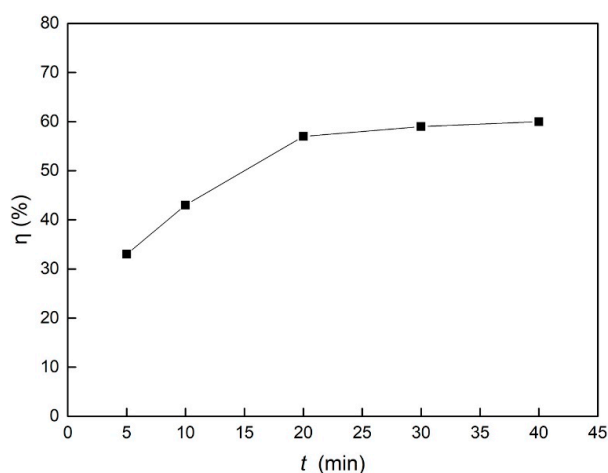
Table 3. Isotherm parameters for the adsorption of catechol on the g-C₃N₄/Fe₃O₄ composite.

| Langmuir Isotherm Parameters | | Freundlich Isotherm Parameters | |
|------------------------------|---------|--------------------------------|--------|
| Q_{\max} (mg/g) | 24.9 | K_F (L/mg) | 0.101 |
| K_L (L/mg) | 0.00134 | n | 1.354 |
| R^2 | 0.9836 | R^2 | 0.9872 |

Figure 8 shows the relationship between the removal rate of catechol and g-C₃N₄/Fe₃O₄ dosage. The removal rate of catechol increased with the increase in material dosage. When the dosage was 50 mg, the removal rate reached 59%. Then, by continuing to increase the amount of g-C₃N₄/Fe₃O₄, the removal rate of catechol remained basically at the same value, which can be attributed to the adsorption equilibrium between g-C₃N₄/Fe₃O₄ and catechol.

**Figure 8.** Effect of g-C₃N₄/Fe₃O₄ dosage on the catechol removal rate.

The relationship between the adsorption time and the removal rate of catechol is shown in Figure 9. It can be seen from the figure that the removal rate of catechol increased continuously with the progress of ultrasonic adsorption. When the adsorption time was 30 min, the removal rate reached 59%. When the ultrasonic adsorption was continued, the adsorption tended to be stable, and the removal rate basically remained at the same value.

**Figure 9.** Effect of adsorption time on the catechol removal rate.

The removal rates of $g\text{-C}_3\text{N}_4/\text{Fe}_3\text{O}_4$ for catechol under different pH were determined and presented in Figure 10, where the removal rate of catechol increased gradually with the increase in the solution pH. At a pH value of 6, the removal rate of catechol reached 70%. Then, with the increase in pH, the removal rate decreased slightly at 7 and 8, while at a pH value of 9, the removal rate decreased significantly. This suggests that the adsorption of catechol by $g\text{-C}_3\text{N}_4/\text{Fe}_3\text{O}_4$ materials may be the result of the interaction between charged groups (as described in Table 4 [26,35,36]). The amine groups on the surface of the $g\text{-C}_3\text{N}_4/\text{Fe}_3\text{O}_4$ act as proton acceptors because of the free lone pair electrons on the nitrogen atom and acquire positive surface charges [36]. At the same time, primary and secondary amine groups react with hydroxyl ions, making the $g\text{-C}_3\text{N}_4/\text{Fe}_3\text{O}_4$ particles negatively charged [26,35]. Under weak acid, weak base, and neutral conditions, catechol mainly presents in its molecular form, so hydrogen bonds are formed between the phenolic hydroxyl groups in catechol and the amino groups in $g\text{-C}_3\text{N}_4/\text{Fe}_3\text{O}_4$ materials, leading to its strong adsorption capacity. However, under strong alkaline conditions, the surfaces of the materials are negatively charged due to their deprotonation, while most of the catechol molecules are ionized, leading to the reduction in the adsorption capacity amount. This could be caused by the electrostatic repulsion between the deprotonated material and ionized catechol, thus affecting the recovery rate of the magnetic solid phase extraction. Suresh et al. [12] reported that the interaction of catechol with granular activated carbon at neutral pH occurred through hydrogen bonding. Moreno-Piraján et al. [13] and Khalfa [14] found that the best adsorption of catechol on activated carbon and dolomite both occurred at pH 7. These reported results of pH are similar to the results in this experiment. Therefore, the optimal pH value of the solution is 6.

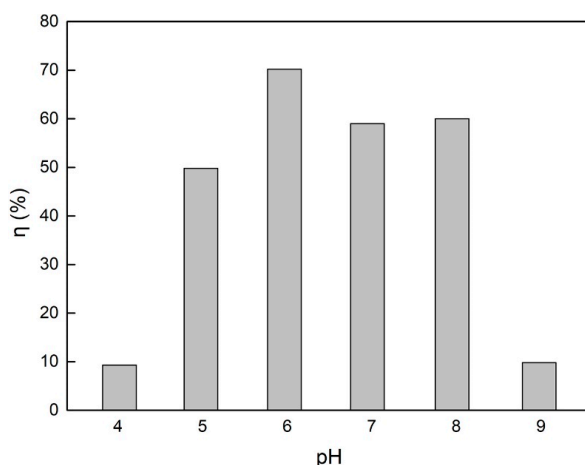


Figure 10. Effect of pH on the catechol removal rate.

Table 4. Equations of the ionization of amine groups on the $g\text{-C}_3\text{N}_4/\text{Fe}_3\text{O}_4$ surface in an aqueous suspension [26,35,36].

| pH of Solutions | Possible Ionization Equations |
|---|--|
| Acid conditions | $\equiv\text{C}-\text{NH}_2 + \text{H}^+ \longrightarrow \equiv\text{C}-\text{NH}_3^+$ |
| | $\begin{array}{c} \equiv\text{C} \\ \diagdown \\ \text{NH} \\ \diagup \\ \equiv\text{C} \end{array} + \text{H}^+ \longrightarrow \begin{array}{c} \equiv\text{C} \\ \diagdown \\ \text{NH}_2^+ \\ \diagup \\ \equiv\text{C} \end{array}$ |
| | $\begin{array}{c} \equiv\text{C} \\ \diagdown \\ \text{N} \\ \diagup \\ \equiv\text{C} \end{array} + \text{H}^+ \longrightarrow \begin{array}{c} \equiv\text{C} \\ \diagdown \\ \text{NH}^+ \\ \diagup \\ \equiv\text{C} \end{array}$ |
| | $\equiv\text{C}-\text{NH}_2 + \text{H}_2\text{O} \longrightarrow \equiv\text{C}-\text{OH} + \text{NH}_3$ |
| | $\equiv\text{C}-\text{OH} + \text{H}^+ \longrightarrow \equiv\text{C}-\text{OH}_2^+$ |
| | Base conditions |
| $\begin{array}{c} \equiv\text{C} \\ \diagdown \\ \text{NH} \\ \diagup \\ \equiv\text{C} \end{array} + \text{OH}^- \longrightarrow \begin{array}{c} \equiv\text{C} \\ \diagdown \\ \text{N}^- \\ \diagup \\ \equiv\text{C} \end{array} + \text{H}_2\text{O}$ | |
| $\equiv\text{C}-\text{OH} + \text{OH}^- \longrightarrow \equiv\text{C}-\text{O}^- + \text{H}_2\text{O}$ | |

3.3. Desorption of Catechol

Acetonitrile, methanol, and isopropanol were added as desorption agents to investigate the desorption capacities for catechol. As can be seen from Figure 11, the desorption rates of the three desorbents were not very low, most likely due to their similar high polarity to catechol and the presence of the lone pairs of electrons, which is beneficial to the affinity of catechol. Among the three desorption agents, methanol had the highest recovery rate of 82%, followed by isopropanol with a recovery rate of 72%, and acetonitrile had the lowest recovery rate of 49%. This might be because methanol and isopropanol possess hydroxyl groups that can form hydrogen bonds with catechol, which is more easily eluted than acetonitrile. Therefore, methanol was selected as the desorption agent in this work.

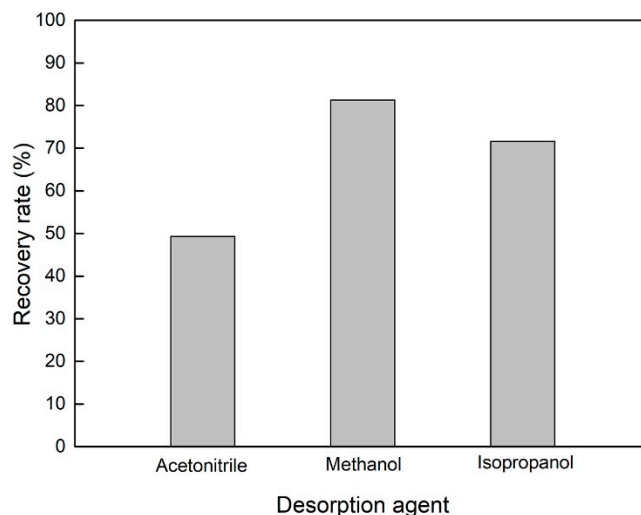


Figure 11. Effect of desorption agent on the recovery of catechol.

To investigate the recyclability of $g\text{-C}_3\text{N}_4/\text{Fe}_3\text{O}_4$, five adsorption and desorption experiments were developed under the optimum conditions obtained earlier. As shown in Figure 12, after five cycles, the removal rate of catechol by the $g\text{-C}_3\text{N}_4/\text{Fe}_3\text{O}_4$ composite remained at about 70%, which indicates that the material has good stability and reusability.

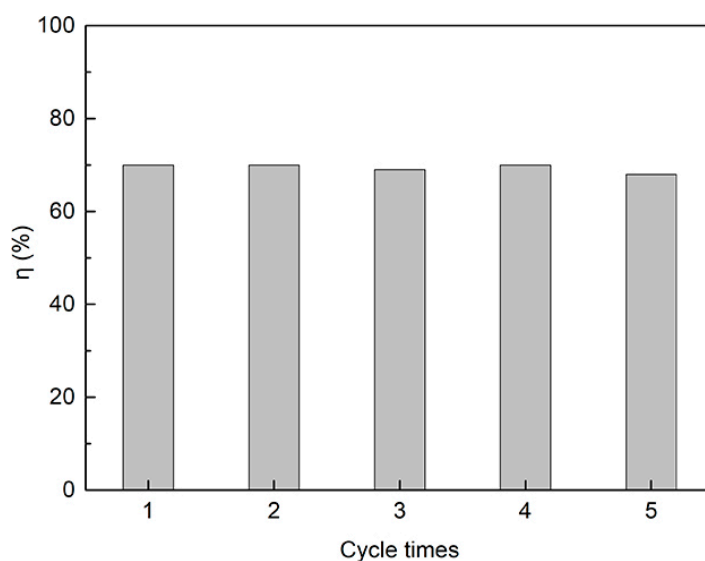


Figure 12. The reusability of the $g\text{-C}_3\text{N}_4/\text{Fe}_3\text{O}_4$ composite.

3.4. Comparison with Other Adsorbents

The maximum adsorption capacity (Q_m), contact time (t_e), and the BET surface area (S_{BET}) of different adsorbents toward catechol are listed in Table 5. The results show that g-C₃N₄/Fe₃O₄ takes a comparatively shorter time to reach the equilibrium than other adsorbents such as activated carbon, modified dolomite, hydroxyapatite, α -alumina, magnetic vermiculite, resin, and waste Fe(III)/Cr(III) hydroxide. The quick adsorption on g-C₃N₄/Fe₃O₄ suggests that it has a very high adsorption efficiency of catechol from water in unit time. Furthermore, compared with other adsorbents, the presence of Fe₃O₄ on the g-C₃N₄/Fe₃O₄ composite makes the separation of catechol from water very rapidly by an external magnetic field, which greatly simplifies the cumbersome procedures such as centrifugation and filtration. Therefore, this reusable g-C₃N₄/Fe₃O₄ composite appears to be very effective and shows significant potential for removing catechol from water.

Table 5. Comparison of the adsorption performances of different adsorbents for catechol.

| Adsorbent | Q_m (mg/g) | t_e | S_{BET} (m ² /g) | Ref. |
|---|--------------|---------|-------------------------------|-----------|
| Granular activated carbon | 977.6 | 12 h | 855 | [12] |
| Activated carbon | 238.10 | 48 h | 1140 | [13] |
| Modified dolomite | 74.1 | 120 min | 31.39 | [14] |
| Modified montmorillonite | 103.5796 | 30 min | - | [15] |
| Hydroxyapatite | 15 | 120 min | 145 | [16] |
| Organophilic-bentonite | 51.97 | 45 min | - | [17] |
| α -alumina | 2.4 | 60 min | - | [21] |
| Magnetic vermiculite | 75 | 240 min | 37.5 | [22] |
| Resin | 160.75 | 150 min | - | [23] |
| Waste Fe(III)/Cr(III) hydroxide | 4.0 | 100 min | 156 | [24] |
| g-C ₃ N ₄ /Fe ₃ O ₄ | 24.9 | 30 min | 38.8 | This work |

4. Conclusions

In this work, g-C₃N₄/Fe₃O₄ magnetic nanocomposite was successfully prepared by chemical co-precipitation and used as the adsorbent to separate catechol from water for the first time, presenting good adsorption properties such as considerably high capacity and short adsorption equilibrium time. More importantly, the g-C₃N₄-Fe₃O₄ nanocomposite could be recovered by an external magnetic field and reused without reducing the adsorption performance, even after five successive cycles. Therefore, g-C₃N₄-Fe₃O₄ nanocomposite is a promising material for the removal of catechol from water.

Author Contributions: Conceptualization, R.X. and Y.P.; Investigation, R.X.; Supervision, Y.P.; Writing—original draft, R.X.; Writing—review & editing, Y.P.

Funding: This research was supported by the Natural Science Foundation of Jiangxi Provincial Department of Education, China (GJJ161129), the Natural Science Foundation of Jiangxi Province, China (20161BAB213062), and the National Natural Science Foundation of China (21506088, 21868017).

Conflicts of Interest: The authors declare no conflicts of interest.

References

- Gulley-Stahl, H.; Hogan, P.A.; Schmidt, W.L.; Wall, S.J.; Buhrlage, A.; Bullen, H.A. Surface Complexation of Catechol to MetalOxides: An ATR-FTIR, Adsorption, and Dissolution Study. *Environ. Sci. Technol.* **2010**, *44*, 4116–4121. [[CrossRef](#)] [[PubMed](#)]
- Environment Canada and Health Canada. *Priority Substances List Assessment Report: 1,2-Dihydroxybenzene*; Canadian Environmental Protection Act: Ottawa, ON, Canada, 1993.
- Moeder, M. Phenols Analysis in Environmental Samples. In *Encyclopedia of Analytical Chemistry*; John Wiley & Sons, Ltd.: Hoboken, NJ, USA, 2006.

4. Gogate, P.R. Treatment of wastewater streams containing phenolic compounds using hybrid techniques based on cavitation: A review of the current status and the way forward. *Ultrason. Sonochem.* **2008**, *15*, 1–15. [[CrossRef](#)] [[PubMed](#)]
5. Wang, Y.; Zhang, S.; Dong, Y.; Qu, J.Y. Research progress of methods for detecting catechol and hydroquinone in water. *Chem. Res.* **2015**, *26*, 100–104.
6. Wang, Q.Q.; Cui, J.; Li, G.H.; Zhang, J.N.; Li, D.W.; Huang, F.L.; Wei, Q.F. Laccase Immobilized on a PAN/Adsorbents Composite Nanofibrous Membrane for Catechol Treatment by a Biocatalysis/Adsorption Process. *Molecules* **2014**, *19*, 3376–3388. [[PubMed](#)]
7. Tušek, A.J.; Šalić, A.; Zelić, B. Catechol Removal from Aqueous Media Using Laccase Immobilized in Different Macro- and Microreactor Systems. *Appl. Biochem. Biotechnol.* **2017**, *182*, 1575–1590. [[CrossRef](#)] [[PubMed](#)]
8. Aghapour, A.A.; Moussavi, G.; Yaghmaeian, K. Degradation and COD removal of catechol in wastewater using the catalytic ozonation process combined with the cyclic rotating-bed biological reactor. *J. Environ. Manag.* **2015**, *157*, 262–266. [[CrossRef](#)] [[PubMed](#)]
9. Su, C.Y.; Lu, Y.X.; Deng, Q.J.; Chen, S.L.; Pang, G.G.; Chen, W.Y.; Chen, M.L.; Huang, Z. Performance of a novel ABR-bioelectricity-Fenton coupling reactor for treating traditional Chinese medicine wastewater containing catechol. *Ecotoxicol. Environ. Saf.* **2019**, *177*, 39–46. [[CrossRef](#)]
10. Yang, X.F.; He, J.; Sun, Z.X.; Holmgren, A.; Wang, D.S. Effect of phosphate on heterogeneous Fenton oxidation of catechol by nano-Fe₃O₄: Inhibitor or stabilizer. *J. Environ. Sci.* **2016**, *39*, 69–76. [[CrossRef](#)] [[PubMed](#)]
11. Li, W.G.; Wang, Y.; Irini, A. Effect of pH and H₂O₂ dosage on catechol oxidation in nano-Fe₃O₄ catalyzing UV-Fenton and identification of reactive oxygen species. *Chem. Eng. J.* **2014**, *244*, 1–8. [[CrossRef](#)]
12. Suresh, S.; Srivastava, V.C.; Mishra, I.M. Study of Catechol and Resorcinol Adsorption Mechanism through Granular Activated Carbon Characterization, pH and Kinetic Study. *Sep. Sci. Technol.* **2011**, *46*, 1750–1766. [[CrossRef](#)]
13. Moreno-Piraján, J.C.; Blanco, D.; Giraldo, L. Relation Between the Adsorbed Quantity and the Immersion Enthalpy in Catechol Aqueous Solutions on Activated Carbons. *Int. J. Mol. Sci.* **2012**, *13*, 44–55. [[CrossRef](#)] [[PubMed](#)]
14. Khalfa, A.; Mellouk, S.; Khelifa, K.M.; Khelifa, A. Removal of catechol from water by modified dolomite: Performance, spectroscopy, and mechanism. *Water Sci. Technol.* **2018**, *77*, 1920–1930. [[PubMed](#)]
15. Liu, Y.N.; Gao, M.L.; Gu, Z.; Luo, Z.X.; Ye, Y.G.; Lu, L.F. Comparison between the removal of phenol and catechol by modified montmorillonite with two novel hydroxyl-containing Gemini surfactants. *J. Hazard. Mater.* **2014**, *267*, 71–80. [[CrossRef](#)] [[PubMed](#)]
16. Sebei, H.; Minh, D.P.; Lyczko, N.; Sharrock, P.; Nzihou, A. Hydroxyapatite-based sorbents: Elaboration, characterization and application for the removal of catechol from the aqueous phase. *Environ. Technol.* **2016**, *38*, 2611–2620. [[PubMed](#)]
17. Shakir, K.; Ghoneimy, H.F.; Elkafrawy, A.F.; Beheir, S.G.; Refaat, M. Removal of catechol from aqueous solutions by adsorption onto organophilic-bentonite. *J. Hazard. Mater.* **2018**, *150*, 765–773. [[CrossRef](#)] [[PubMed](#)]
18. Saikia, N.; Sarma, J.; Borah, J.M.; Mahiuddin, S. Adsorption of 3,4-dihydroxybenzoic acid onto hematite surface in aqueous medium: Importance of position of phenolic-OH groups and understanding of the same using catechol as an auxiliary model. *J. Colloid Interface Sci.* **2013**, *398*, 227–233. [[CrossRef](#)] [[PubMed](#)]
19. Yang, Y.L.; Yan, W.; Jing, C.Y. Dynamic Adsorption of Catechol at the Goethite/Aqueous Solution Interface: A Molecular-Scale Study. *Langmuir* **2012**, *28*, 14588–14597. [[PubMed](#)]
20. Kristoffersen, H.H.; Shea, J.E.; Metiu, H. Catechol and HCl Adsorption on TiO₂(110) in Vacuum and at the Water-TiO₂ Interface. *J. Phys. Chem. Lett.* **2015**, *6*, 2277–2281.
21. Borah, J.M.; Sarma, J.; Mahiuddin, S. Adsorption comparison at the α -alumina/water interface: 3,4-Dihydroxybenzoic acid vs. catechol. *Colloids Surf. A Physicochem. Eng. Asp.* **2011**, *387*, 50–56. [[CrossRef](#)]
22. Chen, W.X.; Li, Q.; Yan, J.J.; Zhu, Z.H.; Wang, X.L.; Zhou, X.H. Research on the adsorption capability of CTMAB-magnetic vermiculite for catechol. *Ind. Water Treat.* **2019**, *39*, 58–61.
23. Li, H.P.; Lin, L.Z.; Feng, Y.Z.; Zhao, M.M.; Li, X.T.; Zhu, Q.Y.; Xiao, Z.B. Enrichment of antioxidants from soy sauce using macroporous resin and identification of 4-ethylguaiacol, catechol, daidzein, and 4-ethylphenol as key small molecule antioxidants in soy sauce. *Food Chem.* **2018**, *240*, 885–892. [[CrossRef](#)] [[PubMed](#)]

24. Namasivayam, C.; Sumithra, S. Adsorptive removal of catechol on waste Fe(III)/Cr(III) hydroxide: Equilibrium and kinetics study. *Ind. Eng. Chem. Res.* **2004**, *43*, 7581–7587. [[CrossRef](#)]
25. Thomas, A.; Fischer, A.; Goettmann, F.; Antonietti, M.; Müller, J.O.; Schlögl, R.; Carlsson, J.M. Graphitic carbon nitride materials: Variation of structure and morphology and their use as metal-free catalysts. *J. Mater. Chem.* **2008**, *18*, 4893–4908. [[CrossRef](#)]
26. Sun, Y.P.; Ha, W.; Chen, J.; Qi, H.Y.; Shi, Y.P. Advances and applications of graphitic carbon nitride as sorbent in analytical chemistry for sample pretreatment: A review. *Trend. Anal. Chem.* **2016**, *84*, 12–21. [[CrossRef](#)]
27. Nian, Q.X.; Liu, Y.M.; Sun, B.; Wang, M.M. Determination of three hydroxyl polycyclic aromatic hydrocarbons in urine using magnetic solid-phase extraction with magnetic carbon nitride composites coupled with high performance liquid chromatography. *Chin. J. Chromatogr.* **2019**, *37*, 252–258. [[CrossRef](#)]
28. Wang, M.; Cui, S.H.; Yang, X.D.; Bi, W.T. Synthesis of g-C₃N₄/Fe₃O₄ nanocomposites and application as a new sorbent for solid phase extraction of polycyclic aromatic hydrocarbons in water samples. *Talanta* **2015**, *132*, 922–928. [[CrossRef](#)] [[PubMed](#)]
29. Kumar, S.; Surendar, T.; Kumar, B.; Baruah, A.; Shanker, V. Synthesis of magnetically separable and recyclable g-C₃N₄-Fe₃O₄ hybrid nanocomposites with enhanced photocatalytic performance under visible-light irradiation. *J. Phys. Chem. C* **2013**, *117*, 26135–26143. [[CrossRef](#)]
30. Liang, Q.Q.; Yu, L.H.; Jiang, W.; Zhou, S.; Zhong, S.T.; Jiang, W. One-pot synthesis of magnetic graphitic carbon nitride photocatalyst with synergistic catalytic performance under visible-light irradiation. *J. Photochem. Photobiol. A* **2017**, *335*, 165–173. [[CrossRef](#)]
31. Zhou, X.S.; Jin, B.; Chen, R.Q.; Peng, F.; Fang, Y.P. Synthesis of porous Fe₃O₄/g-C₃N₄ nanospheres as highly efficient and recyclable photocatalysts. *Mater. Res. Bull.* **2013**, *48*, 1447–1452. [[CrossRef](#)]
32. Zheng, H.B.; Ding, J.; Zheng, S.J.; Zhu, G.T.; Yuan, B.F.; Feng, Y.Q. Facile synthesis of magnetic carbon nitride nanosheets and its application in magnetic solid phase extraction for polycyclic aromatic hydrocarbons in edible oil samples. *Talanta* **2016**, *148*, 46–53. [[CrossRef](#)]
33. Langmuir, I. Adsorption of gases on plane surfaces of glass, mica and platinum. *J. Am. Chem. Soc.* **1918**, *40*, 1361–1403. [[CrossRef](#)]
34. Freundlich, H.M.F. Over the adsorption in solution. *J. Phys. Chem.* **1906**, *57*, 385–470.
35. Singh, B.; Gaydardzhiev, S.; Ay, P. Stabilization of aqueous silicon nitride suspension with Dolapix A88. *J. Dispers. Sci. Technol.* **2006**, *27*, 91–97. [[CrossRef](#)]
36. Zhu, B.; Xia, P.; Ho, W.; Yu, J. Isoelectric point and adsorption activity of porous g-C₃N₄. *Appl. Surf. Sci.* **2015**, *344*, 188–195. [[CrossRef](#)]



© 2019 by the authors. Licensee MDPI, Basel, Switzerland. This article is an open access article distributed under the terms and conditions of the Creative Commons Attribution (CC BY) license (<http://creativecommons.org/licenses/by/4.0/>).